ELSEVIER

Journal of Nuclear Materials 278 (2000) 290–300

journal of nuclear materials

www.elsevier.nl/locate/jnucmat

$KNa_3(UO_2)_2(Si_4O_{10})_2(H_2O)_4$, a new compound formed during vapor hydration of an actinide-bearing borosilicate waste glass

Peter C. Burns [a,*], Rudolph A. Olson [b], Robert J. Finch [b], John M. Hanchar [a,1], Yves Thibault [c]

[a] *Department of Civil Engineering and Geological Sciences, University of Notre Dame, 156 Fitzpatrick, Notre Dame, IN 46556-0767, USA*

[b] *Chemical Technology Division, Argonne National Laboratory, 9700 South Cass Ave., Argonne, IL 60439, USA*

[c] *Department of Earth Sciences, University of Western Ontario, London, Ont., Canada N6A 5B7*

Received 29 June 1999; accepted 15 September 1999

Abstract

Vapor hydration experiments on a U-doped borosilicate waste glass at 200°C produced a novel uranium silicate. Single crystal X-ray structure analysis of this phase indicate the ideal formula $KNa_3(UO_2)_2(Si_4O_{10})_2(H_2O)_4$, although the compound shows some compositional variability. It is monoclinic, space group $C2$, $Z = 2$, $a = 1.2782(1)$, $b = 1.3654(1)$, $c = 0.82677(8)$ nm, $\beta = 119.240(1)°$. The structure was solved by direct methods and refined to an agreement index (R) of 3.6% for 2239 unique observed ($|F_0| \geqslant 4\sigma_F$) reflections and a goodness-of-fit of 1.05. The structure contains vertex-sharing silicate tetrahedra arranged in four and eight-membered rings that are linked to give sheets parallel to (0 0 1). The sheets are cross-linked by vertex-sharing with UrO_4 square bipyramids [$Ur = (UO_2)^{2+}$ uranyl ion], forming a framework of polyhedra of higher bond-valence. The title phase is the major sink for U during glass corrosion at 200°C after approximately 60 days in a saturated vapor environment. Consideration of the structural sites reveals the potential of this compound to incorporate radionuclides from a variety of nuclear-waste glasses over a wide range of environmental conditions.

1. Introduction

High-level waste sludges containing uranium and trace amounts of the other actinides are currently being immobilized in borosilicate glass at the Savannah River Site. In the course of studying reactions of borosilicate waste glass with water vapor, we discovered an apparently new uranium silicate material that formed as an alteration product on the surface of a vapor-hydrated glass. Analysis of this phase by scanning electron microscopy with energy-dispersive X-ray spectroscopy (SEM/EDS) indicated a composition similar to that of Na-weeksite $Na_2(UO_2)_2(Si_2O_5)_3{\cdot}4H_2O$; however, the crystal habit was inconsistent with that of weeksite-group minerals [1] (Fig. 1). The X-ray powder diffraction pattern does not match that of any known solid and subsequent X-ray diffraction analyses of a single crystal verified that this compound is new to science. It was first observed after 35 days of reaction at 200°C and 100% relative humidity, and by 60 days was the predominant uranium-bearing solid on the surface of the glass, a result that may have important implications for the long-term performance of actinide-bearing waste glasses.

2. Background

Yucca Mountain, Nevada, is proposed as the site for the US repository for high-level nuclear waste glasses, which are designed to endure a wide range of hydro-

* Corresponding author. Tel.: +1-219 631 7380; fax: +1-219 631 9236.

E-mail addresses: pburns@nd.edu (P.C. Burns), jhanch@gwu.edu (J.M. Hanchar).

[1] Present address: Department of Geology, The George Washington University, Washington, DC 20052, USA.

0022-3115/00/$ - see front matter
PII: S0022-3115(99)00247-0

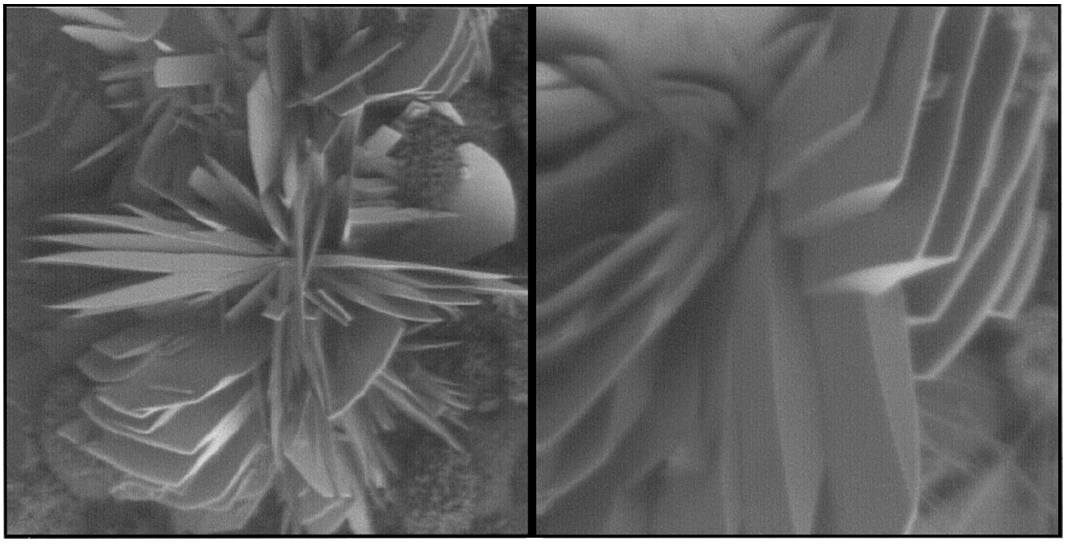

Fig. 1. Backscatter scanning electron micrograph of KNAURSI found on the surface of 51S waste glass subjected to vapor hydration for 60 days at 200°C and 100% RH. Field of view = 328 μm.

logical conditions for long periods of time. One type of glass under consideration by the US Department of Energy for use in such a repository is borosilicate glass. Borosilicate waste glasses can react with water vapor at appreciable rates, depending on environmental conditions [2–4]. The proposed repository will be located above the current water table in the unsaturated zone where glass–water interactions may occur primarily within a thin film of liquid water condensed on the glass surface. During the first 300–1000 yr after the repository is closed, temperatures within will probably remain above 100°C due to heat generated by radioactive decay. When the temperature drops below the boiling point of water, the extent of glass hydration may already be considerable. This is important because liquid water does not interact with pre-hydrated glasses in the same way that it interacts with pristine glasses. Bates et al. [5] showed that pre-hydrated waste glasses release actinides up to 185 times faster than unaltered waste glasses. Therefore, understanding the mechanisms and kinetics of vapor hydration is essential to predict the long-term performance of borosilicate nuclear waste glasses and the extent of hydration at the time liquid water contacts the glass. Towards this goal, we have been measuring the extent of glass hydration in water vapor as a function of time, temperature, and glass composition.

The reaction between water vapor and glass includes the loss of certain elements from the glass and concomitant hydrolysis of the glass-forming network (e.g., alkali metal ions in the glass may exchange with H_3O^+ in solution [6,7]). During reaction in water vapor, a thin film of water on the glass surface rapidly supersaturates with respect to crystalline alteration products, such as zeolites or clay minerals, depending on pH [2–4]. Identification of these alteration products and of their paragenesis helps to characterize mechanisms that may control rates of glass hydration [2–4] and radionuclide release.

3. Experimental and analytical procedures

3.1. Glass preparation

The composition of the glass (designated 51S) that reacted to form the new K–Na uranyl silicate (hereafter designated KNAURSI) is given in Table 1. The glass was synthesized by melting reagent-grade oxides in a Pt/Rh crucible at 1150°C for 4 h and then pouring the melt into a pan of water. The resulting frit was crushed until it passed through a 20 mesh sieve. The frit was re-melted at 1150°C for 4 h, poured into a Pt/Au boat, and annealed at 550°C for 2 h. At the end of the 2 h anneal, the oven was turned off and allowed to cool overnight to room temperature. Back-scattered electron (BSE) analyses in a scanning electron microscope (SEM) showed the glass to be homogeneous. The annealed glass was wet-cored and sliced to obtain 1 cm-diameter by 1 mm-thick disks. Disks were notched, polished with 600-grit SiC under ethyl alcohol, and ultrasonically cleaned in ethyl alcohol.

3.2. Vapor hydration experiments

Several vapor hydration tests were performed at 200°C for various reaction times between 3 and 60 days.

Table 1
Composition of 51S glass (wt%)

SiO_2	54.67
B_2O_3	7.29
Al_2O_3	5.11
P_2O_5	0.56
Cr_2O_3	0.43
Na_2O	9.30
Li_2O	4.41
K_2O	1.36
CaO	1.34
FeO	10.68
MgO	1.74
MnO	1.11
NiO	0.26
ZnO	0.12
La_2O_3	0.52
UO_2	1.07
TiO_2	0.02
ThO_2	0.01

Two polished glass disks were suspended by a Teflon™ thread from a stainless steel hanger inserted into a 22 ml, 304 l stainless-steel Parr™ reaction vessel. To ensure a saturated environment at 200°C, 0.25 ml of de-ionized water was added to the vessel. Upon termination, vessels were cooled to room temperature; the glass disks were removed and examined by SEM.

3.3. X-ray powder diffraction

Crystals and clusters of crystals of KNAURSI were removed by hand from the surface of a 60-day reacted glass using a tungsten needle. Owing to the presence of intimately intergrown crystals of other phases, including weeksite, $K_2(UO_2)_2(Si_2O_5)_3(H_2O)_4$, and tobermorite, $Ca_5Si_6O_16(OH)_2 \cdot nH_2O$, we could not obtain a large volume of single-phase material for analysis by powder diffraction. Careful separation under an optical microscope assured that most (>90 vol.%) of the material analyzed was KNAURSI. Approximately 100 μg of powder was held by a small amount of rubber cement in the center of a low-background sample holder consisting of an oriented single crystal of Si. X-ray intensity data were collected on a Rigaku Miniflex™ diffractometer using Ni-filtered Cu-Kα radiation ($\lambda = 0.15418$ nm) and a variable-width receiving slit. Data were collected over the range $5° < 2\theta < 65°$ using steps of 0.02° and a counting time of 24 s per step.

Measured *d*-spacings are compared with *d*-spacings calculated from the crystal structure in Table 2. The small amount of material analyzed resulted in low peak-to-background ratios. Peak positions and intensities are therefore subject to potentially large (though undetermined) uncertainties. Because XRD powder data were collected with a variable-width slit, measured intensities do not agree with calculated intensities. Unfortunately, very low intensities due to the small sample size prevented us from adequately re-calculating intensities for a fixed-slit configuration.

3.4. X-ray single-crystal diffraction

Several aggregates of crystals were broken and studied optically, but it was impossible to locate a crystal that exhibited uniform optical properties, and intergrown crystals were too small to be separated. A crystal that showed relatively superior optical properties was mounted on a Bruker PLATFORM 3-circle goniometer equipped with a 1K SMART charge-coupled device (CCD) detector and a crystal-to-detector distance of 5 cm [8].

A complete sphere of data was collected by using monochromatic MoKα X-radiation and frame widths of 0.3° in ω, with 60 s used to acquire each frame. Several hundred frames of data were analyzed, giving 887 diffraction maxima for the determination of the unit-cell parameters (Table 3). It was impossible to index all reflections using only one orientation, indicating that the crystal selected was not a single crystal. Two orientations were identified that accounted for 803 of the 887 reflections, both of which provided identical unit-cell parameters. The stronger of these two groups of reflections accounted for 517 of the reflections collected, and provided unit-cell dimensions and an orientation matrix that were used for the ensuing data reduction. The unit cell of the second, weaker group of reflections was rotated ~7° to the first. Data are consistent with a monoclinic *C*-centered unit cell with dimensions $a = 1.2782(1)$, $b = 1.3654(1)$, $c = 0.82677(8)$ nm, $\beta = 119.240(1)°$, which were refined by least-squares techniques. Data were collected over the range $3° \leqslant 2\theta \leqslant 56.7°$ in approximately 44 h; comparison of the intensities of equivalent reflections collected at different times during the data collection showed no decay. Three-dimensional data were integrated and corrected for Lorentz, polarization, and background effects using the Bruker program SAINT. An empirical absorption correction was done using 2253 intense reflections and modeling the crystal as a plate; reflections with a plate-glancing angle less than 3° were discarded from consideration, and the absorption correction lowered R_{INT} for the remaining reflections from 14.6% to 5.3%. A total of 13 584 reflections remained after omitting reflections with a plate-glancing angle less that 3°. Of the reflections collected, 6811 are consistent with a *C*-centered lattice. Merging equivalent reflections left 3004 unique reflections ($R_{INT} = 5.4\%$) with 2239 classed as observed ($|F_0| \geqslant 4\sigma_F$).

Table 2
X-ray powder-diffraction data for $KNa_3(UO_2)_2[Si_4O_{10}]_2(H_2O)_4$[a]

h	*k*	*l*	*d* (calc, nm)	*d* (obs, nm)	I/I_0 (calc)	I/I_0 (obs)
0	0	1	0.7215	0.731	20	7
0	2	0	0.6827	0.685	100	9
−2	0	1	0.6076		25	
2	0	0	0.5577	0.559	35	38
0	2	1	0.4959	0.510	42	3
−2	2	1	0.4539		52	
2	2	0	0.4319	0.4308	18	5
−2	0	2	0.4067	0.4067	23	59
2	0	1	0.3636		10	
0	0	2	0.3607	0.3638	21	100
−2	2	2	0.3494	0.3498	41	4
0	4	0	0.3413		8	
2	2	1	0.3209	0.3195	48	6
0	2	2	0.3189		19	
−4	0	1	0.3174		18	
0	4	1	0.3086		17	
−2	4	1	0.29760	0.2942	30	3
−4	2	1	0.28781	0.2875	19	28
4	0	0	0.27883		16	
−2	0	3	0.27501	0.2754	3	8
−2	4	2	0.26148	0.2608	24	6
4	2	0	0.25813	0.2580	15	45
−4	0	3	0.25331	0.2531	5	8
2	4	1	0.24886	0.2498	10	4
0	4	2	0.24794	0.2485	8	5
−4	2	3	0.23749		12	
2	2	2	0.23634	0.2367	3	5
0	2	3	0.22682	0.2265	7	4
0	6	1	0.21703		8	
−2	4	3	0.21415		11	
−4	0	4	0.20338	0.2034	3	3
2	4	2	0.20270		9	
−2	6	2	0.19860	0.1970	8	6
2	6	1	0.19290	0.1929	4	4
4	0	2	0.18179	0.1819	5	87
−6	4	2	0.18066		14	
6	2	0	0.17936	0.1791	5	8
−2	4	4	0.17454	0.1746	9	4
6	4	0	0.16325	0.1630	3	5
−4	2	5	0.16063	0.1608	2	3
4	4	2	0.16045	0.1601	4	4
−6	4	4	0.15988	0.1596	3	4
−2	2	5	0.15570	0.1556	2	3
0	8	2	0.15428	0.1545	2	3
−6	2	5	0.15304	0.1531	3	4
−8	2	4	0.14828	0.1483	4	4
2	2	4	0.14774	0.1477	3	5
6	4	1	0.14629	0.1462	3	3
0	0	5	0.14429	0.1446	3	4

[a] Cu-K_α radiation ($\lambda = 0.15418$ nm).

3.5. Structure solution and refinement

Scattering curves for neutral atoms, together with anomalous dispersion corrections, were taken from International Tables for X-Ray Crystallography, Vol. IV [9]. The Bruker SHELXTL Version 5 system of programs was used for the determination and refinement of the crystal structure.

Systematic absences and reflection statistics indicated space group *C*2, with verification provided by successful solution and refinement of the structure. The structure was solved by direct methods, and the initial model

Table 3
Miscellaneous information concerning the crystal structure of $KNa_3[(UO_2)(Si_4O_{10})]_2(H_2O)_4$

a (nm)	1.2782(1)	Total ref.	6811
b (nm)	1.3654(1)	Unique ref.	3004
c (nm)	0.82677(8)	R_{int} (%)	5.4
β (°)	119.240(1)	Unique $\lvert F_0\rvert \geqslant 4\sigma_F$	2239
V (Å^3)	125.91(2)	Final R (%)	3.6
Space group	$C2$	S	1.05
$F(0\,0\,0)$	1160		
μ (mm^{-1})	13.56		
D_{calc} (g/cm^3)	3.336		

Unit-cell contents: $2\{KNa_3[(UO_2)(Si_4O_{10})]_2(H_2O)_4\}$
$r = \sum(|F_0| - |F_c|)/\sum|F_0|$
$S = [\sum w(|F_0| - |F_c|)^2/(m-n)]^-$ for m observations and n parameters

included the positions of the U atoms and some of the cations. The remaining cations and the anions were located in successive difference-Fourier maps that were calculated after refinement of the model. The agreement factor (R) for a model that included all atomic positional parameters, the occupancy factors for selected cations, and that accounted for isotropic displacement of all atoms was 4.4% for observed reflections. Displacement parameters for U, K and Na atoms were converted to anisotropic forms, and were refined together with positional parameters for all atoms and a weighting scheme of the structure factors. The final model gave an R index of 3.6% for 2239 unique observed reflections ($|F_0| \geqslant 4\sigma_F$) and a goodness-of-fit (S) of 1.06. In the final cycle of refinement the average parameter shift/esd was 0.000, and the maximum peaks in the difference-Fourier maps were 2.78 and −1.75 e/Å^3. Final atomic-positional parameters and equivalent-isotropic-displacement parameters are given in Table 4 and selected interatomic distances and angles are given in Table 5.

3.6. Electron probe X-ray microanalyses (EPMA)

X-ray microanalyses were done in wavelength-dispersive spectroscopy (WDS) mode on a JEOL JXA 8600

Table 4
Final atomic parameters for $KNa_3[(UO_2)(Si_4O_{10})]_2(H_2O)_4$

	x	y	z	$^*U_{eq}$[a]
U(1)	0.24989(7)	0.4362(2)	0.4998(1)	122(1)
K	0	0.5529(6)	1/2	396(34)
Na(1)	0.6220(5)	0.6845(8)	0.1339(8)	590(22)
Na(2)	1/2	0.326(1)	1/2	257(71)
Na(3)	1/2	0.795(1)	1/2	424(55)
Si(1)	0.5536(5)	0.4665(3)	0.8720(8)	118(12)
Si(2)	0.2707(5)	0.2998(3)	0.8862(8)	107(11)
Si(3)	0.0544(4)	0.4072(3)	0.8708(7)	77(10)
Si(4)	0.7718(4)	0.5755(3)	0.8854(7)	86(11)
O(1)	0.449(1)	0.449(1)	0.670(2)	247(32)
O(2)	0.0455(8)	0.4225(8)	0.340(1)	97(23)
O(3)	0	0.365(1)	0	133(40)
O(4)	0.3073(4)	0.187(1)	0.9601(7)	114(10)
O(5)	0.224(1)	0.5200(9)	0.650(2)	256(34)
O(6)	0.239(1)	0.556(1)	0.309(2)	312(39)
O(7)	0.271(1)	0.3460(8)	0.358(2)	125(25)
O(8)	0.1501(9)	0.3195(7)	0.899(1)	172(27)
O(9)	0.257(1)	0.3086(8)	0.681(2)	169(28)
O(10)	1/2	0.504(1)	0	167(44)
O(11)	0.6265(9)	0.3643(8)	0.950(2)	107(25)
O(12)	0.6406(8)	0.5510(6)	0.865(1)	88(21)
O(13)	0.122(1)	0.5056(9)	0.961(2)	226(32)
H_2O(14)	0.5281(6)	0.194(1)	0.334(1)	272(18)
H_2O(15)	0.582(1)	0.687(3)	0.433(2)	1102(70)

[a] $^*U_{eq} = U_{eq}$ Å$^2 \times 10^4$.

Table 5
Selected interatomic distances (nm) and angles (°) for $KNa_3[(UO_2)(Si_4O_{10})]_2(H_2O)_4$[a]

U(1)–O(7)	0.181(1)	K–O(2),a	0.245(1)×2
U(1)–O(5)	0.183(1)	K–H_2O(14)b,c	0.249(1)×2
U(1)–O(1)	0.223(1)	K–O(5),a	*0.254(1)*×2
U(1)–O(6)	0.223(1)	⟨K(1)–ϕ⟩	0.249
U(1)–O(9)	0.227(1)		
U(1)–O(2)	*0.229(1)*	Si(1)–O(1)	0.157(1)
⟨U(1)–O_{Ur}⟩	0.182	Si(1)–O(10)h	0.1601(8)
⟨U(1)–O_{eq}⟩	0.225	Si(1)–O(12)	0.162(1)
		Si(1)–O(11)	*0.163(1)*
Na(1)–H_2O(15)	0.276(2)	⟨Si(1)–O⟩	0.161
Na(1)–O(3)l	0.283(2)		
Na(1)–O(8)e	0.282(1)	Si(2)–O(11)i	0.161(1)
Na(1)–O(10)	0.283(2)	Si(2)–O(9)	0.162(1)
Na(1)–O(7)d	0.291(1)	Si(2)–O(8)	0.162(1)
Na(1)–O(5)f	0.295(2)	Si(2)–O(4)	*0.163(1)*
Na(1)–O(12)g	*0.296(1)*	⟨Si(2)–O⟩	0.162
⟨Na(1)–ϕ⟩	0.287		
		Si(3)–O(13)	0.157(1)
Na(2)–O(1),f	0.247(2)×2	Si(3)–O(2)a	0.160(1)
Na(2)–H_2O(14),f	0.240(2)×2	Si(3)–O(8)	0.165(1)
Na(2)–O(7),f	*0.258(1)*×2	Si(3)–O(3)h	*0.1640(8)*
⟨Na(2)–ϕ⟩	0.248	⟨Si(3)–O⟩	0.161
Na(3)–H_2O(15),f	0.204(3)×2	Si(4)–O(6)f	0.157(1)
Na(3)–O(2)b,d	0.242(2)×2	Si(4)–O(4)d	0.163(1)
Na(3)–O(9)b,d	0.287(1)×2	Si(4)–O(12)	0.164(1)
Na(3)–O(8)b,d	*0.292(1)*×2	Si(4)–O(13)i	*0.164(1)*
⟨Na(3)–ϕ⟩	0.256	⟨Si(4)–O⟩	0.162
O(7)–U(1)–O(5)	175.8(7)	O(11)i–Si(2)–O(9)	117.9(6)
O(7)–U(1)–O(1)	88.6(4)	O(11)i–Si(2)–O(8)	105.3(6)
O(7)–U(1)–O(6)	91.8(4)	O(11)i–Si(2)–O(4)	103.3(6)
O(7)–U(1)–O(9)	86.5(5)	O(9)–Si(2)–O(8)	115.8(6)
O(7)–U(1)–O(2)	93.7(4)	O(9)–Si(2)–O(4)	109.0(5)
O(5)–U(1)–O(1)	92.9(5)	O(8)–Si(2)–O(4)	*103.9(5)*
O(5)–U(1)–O(6)	93.0(6)	⟨O–Si(2)–O⟩	109.2
O(5)–U(1)–O(9)	89.6(5)		
O(5)–U(1)–O(2)	84.7(5)	O(13)–Si(3)–O(2)a	111.6(7)
O(1)–U(1)–O(6)	92.6(6)	O(13)–Si(3)–O(8)	110.8(6)
O(1)–U(1)–O(9)	88.8(5)	O(13)–Si(3)–O(3)h	107.6(7)
O(1)–U(1)–O(2)	176.8(5)	O(2)a–Si(3)–O(8)	113.1(6)
O(6)–U(1)–O(9)	177.0(6)	O(2)a–Si(3)–O(3)h	113.1(4)
O(6)–U(1)–O(2)	89.7(5)	O(8)–Si(3)–O(3)h	*99.8(7)*
O(9)–U(1)–O(2)	89.0(4)	⟨O–Si(3)–O⟩	109.3
O(1)–Si(1)–O(10)h	109.5(5)	O(6)f–Si(4)–O(4)d	114.8(6)
O(1)–Si(1)–O(12)	108.4(7)	O(6)f–Si(4)–O(12)	106.6(7)
O(1)–Si(1)–O(11)	108.5(7)	O(6)f–Si(4)–O(13)i	108.6(7)
O(10)h–Si(1)–O(12)	108.3(7)	O(4)d–Si(4)–O(12)	108.2(4)
O(10)h–Si(1)–O(11)	111.3(7)	O(4)d–Si(4)–O(13)i	106.4(6)
O(12)–Si(1)–O(11)	*110.7(5)*	O(12)–Si(4)–O(13)i	*112.3(6)*
⟨O–Si(1)–O⟩	109.4	⟨O–Si(4)–O⟩	109.5

[a] a = $-x,\ y,\ 1-z$; b = $1/2-x,\ y+1/2,\ 1-z$; c = $x-1/2,\ y+1/2,\ z$; d = $x+1/2,\ y+1/2,\ z$; e = $x+1/2,\ y+1/2,\ z-1$; f = $1-x,\ y,\ 1-z$; g = $x,\ y,\ z-1$; h = $x,\ y,\ z+14$; i = $1-x,\ y,\ 2-z$.

electron microprobe. Data were reduced using the Heinrich/Duncumb-Reed correction model provided with the dQant program of Geller Microanalytical Laboratory .

Because the compound is sensitive to the electron beam, operating conditions were chosen in order to minimize alkali migration. All analyses were performed with an accelerating voltage of 15 kV, a probe current of

10 nA, and a beam defocused at 10 μm. Counting times on peak and background were 20 s for Si(Kα), Al(Kα), Ca(Kα), and U(Mα), 15 s for K(Kα), and 10 s for Na (Kα). Oxygen was calculated on the basis of stochiometry using assumed valences of the cations. At these conditions, no significant Na and K decay could be detected. A 100 s energy-dispersive scan indicated no elements with Z greater than eight, other than those reported herein. Only those elements identified in the EDS spectra were subsequently analyzed in WDS because the crystals were too small and deteriorated during analysis (of the elements present in the glass, the potential presence in KNAURSI of Li and B could not be checked by WDS). Analytical EMPA standards used were albite (NaKα, SiKα), corundum (Al-Kα), orthoclase (KKα), diopside (CaKα), and synthetic UO_2 (UMα). Identical analytical conditions were used to analyze both standards and the crystal. Counts on the KKα peak were corrected for overlap with the UMα peak; H_2O was determined by difference.

4. Results

4.1. Crystal habit and optical properties

Fig. 1 shows the typical morphology of KNAURSI. Reacted glasses from experiments conducted for 35 days or more at 200°C commonly display numerous clusters of crystals like that shown. After 60 days of hydration, clusters are typically 100–300 μm across and are readily visible under an optical microscope. Individual crystals display bladed to thin tabular habits. Most crystals are several to a few tens of μm thick, and several tens to approximately 100 μm perpendicular to flattening. Crystals are translucent, pale yellow, and not pleochroic. Their optical character is biaxial negative, with a moderate to large 2V (approximately 40°). Extinction is parallel, with a 90° extinction angle in the plane of flattening. Refractive indices for the two directions normal to flattening are ~1.570 and ~1.562 (measured in white light), so that crystals display low birefringence when viewed in this orientation ($\Delta = 0.008$). Some crystals display undulatory extinction. Parallel intergrowths are common, but twinning was not confirmed. Crystals are brittle, with a hardness similar to that of calcite (three on the Mohs scale), and exhibit imperfect cleavage parallel to the plane of flattening.

4.2. Crystal structure

4.2.1. Cation polyhedra

The structure contains four symmetrically distinct Si sites, each of which is tetrahedrally coordinated by four O atoms. The ⟨Si–O⟩ bond-lengths range from 0.161 to 0.162 nm, and the tetrahedral bond-angles are in the range 109.2–109.5° (Table 5).

There is one symmetrically unique U position, and the polyhedral geometry (Table 5) and bond-valence sum of 6.07 valence units (vu), calculated using the parameters of Burns et al. [10], indicate that all U occurs as U^{6+}, consistent with the pale yellow color of the crystals. As is typical for U^{6+} in crystal structures [10], the U^{6+} ion is strongly bonded to two O atoms at ~0.18 nm, forming a nearly linear uranyl ion $(UO_2)^{2+}$ (designated here as Ur). The U^{6+} cation is also coordinated by four additional O atoms at ~0.22 nm, arranged at the equatorial corners of a square bipyramid. Uranyl ions occur in three coordination polyhedra in crystal structures: square bipyramidal, pentagonal bipyramidal, and hexagonal bipyramidal, with uranyl pentagonal bipyramids being the most common [11]. The $\langle U^{6+}–O_{Ur}\rangle$ bond length of 0.182 nm, and the $\langle U^{6+}–O_{eq}\rangle$ bond length of 0.225 nm compare well with average values of 0.179(3) and 0.228(5) nm, respectively, obtained from numerous well-refined structures [10].

The structure contains four symmetrically distinct alkali cation sites in interstices within the uranyl silicate framework. On the basis of a combination of site-scattering refinement and polyhedral geometries, there is one site that contains mostly K, and three that are dominated by Na. The K site is coordinated by two H_2O groups and four O atoms in a distorted-octahedral arrangement, with a mean bond length of 0.249 nm. Site-occupancy refinement indicates the site is 85(2)% occupied, assuming that K is the only constituent. The expected $^{[6]}$K–O bond-length from sums of effective ionic radii [12] is 0.274 nm, and the scattering at the site indicates the presence of a cation (or vacancies) lighter than K. Incorporation of Na at the site could account for both the shorter bond-lengths and the reduced scattering efficiency.

The Na(1) site is coordinated by six O atoms and one H_2O group, with a mean bond length of 0.287 nm. The site-scattering is consistent with only Na present at the site; refinement of the occupancy using the scattering factor for Na indicated the site is 100(2)% occupied. The site shows substantial positional disorder, as reflected by elongated anisotropic-displacement parameters, and the Na(1) site obtained from the refinement represents an average position.

The Na(2) and Na(3) sites are each 60(4)% occupied by Na, on the basis of site-occupancy refinement using the scattering factor for Na. Na(2) is coordinated by two H_2O groups and four O atoms in a distorted-octahedral arrangement, with a mean bond length of 0.248 nm. The Na(3) site is coordinated by two H_2O groups and six O atoms, with a mean bond length of 0.256 nm. The Na(3)–H_2O(15) bond-length of 0.204(3) nm is shorter than expected. However, the displacement parameter for H_2O(15) is extremely large, indicating

positional disorder is likely. Presumably the H_2O(15) O atom moves away from the Na(3) site when it is locally occupied.

4.2.2. Structural connectivity

Burns et al. [13] proposed a hierarchy of crystal structures containing uranyl polyhedra that was arranged on the basis of the polymerization of those polyhedra of higher bond valence. As with most uranyl phases, the crystal structure of KNAURSI is best understood using the approach of Burns et al. [13]. The structure contains both high- and low-valence cation polyhedra, and the structural roles of these two types of polyhedra are distinct. Consider first the polyhedra of higher bond-valence: the uranyl square bipyramids and silica tetrahedra. The silica tetrahedra are arranged in complex sheets of vertex-sharing tetrahedra (Fig. 2), with each tetrahedron contained within a four-membered ring of tetrahedra. The four-membered rings are in turn linked to four additional four-membered rings by sharing corners, resulting in a complex sheet of tetrahedra that is parallel to (0 0 1), which contains eight-membered rings.

Liebau [14] discussed sheets of silica tetrahedra found in minerals. Although several sheets are known that contain four and eight-membered rings of vertex-sharing tetrahedra, no sheet is shown with the configuration found in the current study. The sheet is most similar to that found in apophyllite, $KCa_4[Si_4O_{10}]_2(F,OH)\cdot 8H_2O$, but it differs in the orientations of adjacent tetrahedra in the four and eight-membered rings.

The uranyl square bipyramids occur between the sheets of silica tetrahedra, and each uranyl polyhedron shares its four equatorial corners with four silicate tetrahedra, two in each adjacent sheet (Fig. 3). The silica tetrahedra that share corners with a single uranyl polyhedron are each members of different four-membered rings in the structural sheets. Uranyl ions are oriented sub-parallel to the sheets, and do not link to the silica tetrahedra. The linkages of silica tetrahedra within the sheets with the uranyl polyhedra between the sheets results in a complex framework of polyhedra of higher bond-valence.

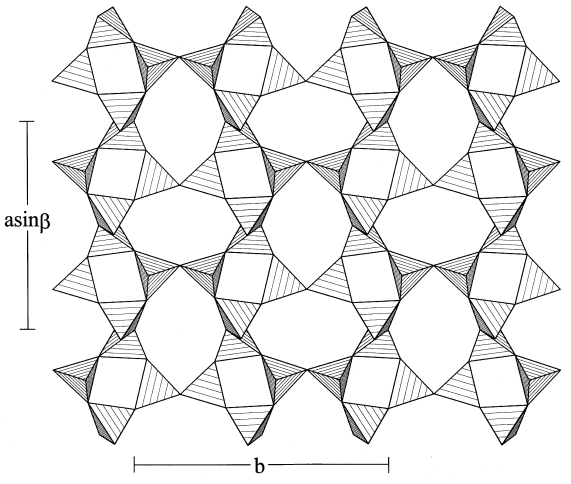

Fig. 2. The sheet of corner-sharing SiO_4 tetrahedra at $c \approx 0$ shown projected along [0 0 1]. The SiO_4 tetrahedra are shown shaded with crosses.

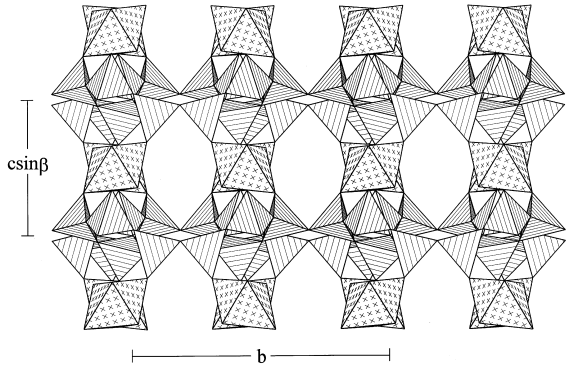

Fig. 3. The framework of KNAURSI projected along [1 0 0]; only the Urϕ_4 pentagonal bipyramids and SiO_4 tetrahedra are shown. Legend as in Fig. 2.

The large, low-valence cations, K^+ and Na^+, and the two symmetrically distinct H_2O groups occupy large voids in the framework (Fig. 4).

4.2.3. Formula of crystal studied

The average of ten electron microprobe analyses is given in Table 6. The empirical formula is $(K_{0.83}Ca_{0.03})Na_{3.21}(UO_2)_{1.80}[Si_{3.96}Al_{0.10}O_{10}]_2(H_2O)_{5.1}$, ideally $KNa_3(UO_2)_2[Si_4O_{10}]_2(H_2O)_5$. This formula agrees well with the composition inferred from the crystal-structure determination: $K_{0.85}Na_{3.20}(UO_2)_2[Si_4O_{10}]_2(H_2O)_4$. EMPA data indicate that Al and Ca are present, although Al is highly variable (Table 6), ranging from 0.257 to 1.488 wt% Al_2O_3 within the crystal analyzed. Aluminum probably occupies Si sites.

The U determined by EMPA is lower than expected on the basis of the structure refinement. A slight deficiency in U may be an artifact of the EMPA analysis. The deficit in the EMPA total in Table 6 requires an overestimate of the weight percent H_2O (2.25 wt%) by an amount comparable to the apparent deficit in UO_3 (3.53 wt%). Because the Mα X-ray line of U is used for microanalysis and the standard (UO_2) is rather dissimilar to KNAURSI in composition, there is a possibility that the deficiency in U is an artifact of the matrix correction.

The uranyl silicate framework of KNAURSI has a net charge of −4 per formula unit (p.f.u), thus the low-valence cations and any anionic species that occur in the

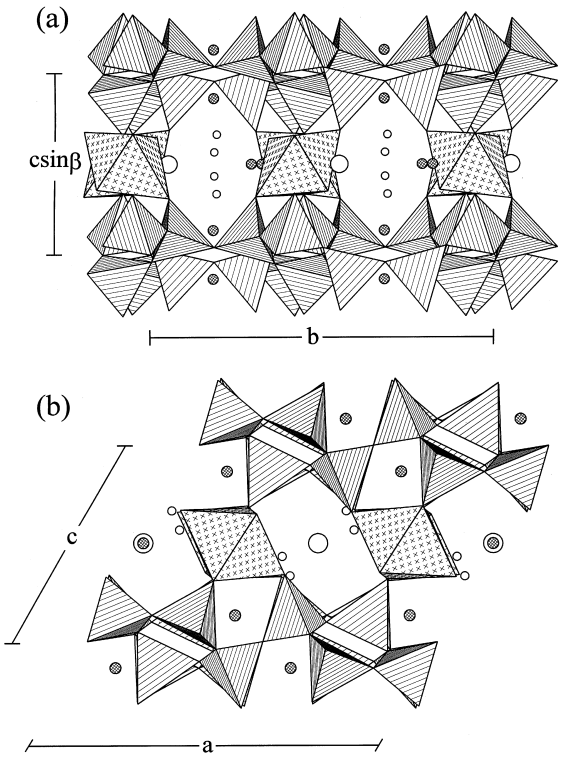

Fig. 4. The structure of KNAURSI showing the locations of K (large open circles), Na (cross-hatched circles) and H_2O (smaller open circles): (a) projected along [1 0 0], (b) projected along [0 1 0].

Table 6
EMPA results for crystal 51Sa compared with ideal compositions based on the crystal structure (wt% oxide)

	EMPA[a]	XRD[b]
Na_2O	8.02 (0.28)	8.04
K_2O	3.17 (0.08)	2.98
CaO	0.13 (0.06)	–
UO_3	41.45 (0.91)	45.25
SiO_2	38.37 (0.34)	38.03
Al_2O_3	0.86 (0.55)	–
H_2O	8.02 (0.56)	5.70

[a] Average of 10 analyses; H_2O calculated by difference. Estimated standard deviations (1σ) are shown in parentheses and represent variability of 10 analyses; analytical precision for each analysis was significantly smaller.
[b] Analytical totals calculated from XRD single-crystal structure analysis; note that XRD cannot distinguish between Ca and K or between Si and Al, so that Ca and Al are not considered.

interstitial sites must have a net charge of +4 pfu. The chemical analysis and structure determination indicate these sites contain K, Na and H_2O, and possibly minor Ca. The K and Na(1) sites are close to fully occupied, whereas the Na(2) and Na(3) sites are ~60% occupied, an observation that can be ascribed to the necessity of electoneutrality. There is no apparent reason why the Na(2) and Na(3) sites cannot be fully occupied, but charge-balance requirements would have to be met, possibly by the K site being vacant. In this case a Na-rich compositional end member results, $Na_4(UO_2)_2(Si_4O_{10})_2(H_2O)_4$, and a solid-solution series between KNAURSI and the Na end member may exist.

4.2.4. Related structures

Most uranyl phases possess structures that are dominated by sheets of edge- and corner-sharing uranyl polyhedra that sometimes also involve other polyhedra of higher bond-valence. This is the case in several uranyl silicates with U:Si ratios of 1:1, including α-uranophane, $Ca[(UO_2)(SiO_3OH)]_2(H_2O)_5$, β-uranophane, $Ca[(UO_2)(SiO_3OH)]_2(H_2O)_5$, boltwoodite, $(K,Na)[(UO_2)(SiO_3OH)](H_2O)_{1.5}$, sklodowskite, $Mg[(UO_2)(SiO_3OH)]_2(H_2O)_6$, cuprosklodowskite, $Cu[(UO_2)(SiO_3OH)]_2(H_2O)_6$, and kasolite, $Pb[(UO_2)(SiO_4)](H_2O)$. The U in each of these structures is in pentagonal bipyramidal coordination, with the uranyl polyhedra sharing edges to form chains. The chains of uranyl polyhedra are cross-linked by sharing edge and vertices with silica tetrahedra, forming uranyl silicate sheets. In each mineral lower-valence cations and H_2O groups occupy interlayer sites, and all but kasolite contain acid silicate groups.

Soddyite is a uranyl silicate phase with a U:Si ratio of 2:1. It has a structure based upon a framework of polymerized polyhedra of higher bond-valence. All U in the soddyite structure is in pentagonal bipyramidal coordination, with uranyl polyhedra linked by sharing edges to form chains, which are in turn linked into a framework by sharing edges with silica tetrahedra.

Haiweeite has a U:Si ratio of 1:3, and involves sheets of uranyl and silica polyhedra. Uranyl pentagonal bipyramids share edges, forming chains one polyhedron wide, with silica tetrahedra attached to each side of the chain by sharing edges. These uranyl silicate chains are cross-linked to form sheets by a crankshaft-like chain of vertex-sharing silica tetrahedra.

It is interesting to note that there are structural trends in uranyl silicates. Those with U:Si ratios 2:1 and 1:1 do not involve polymerization of the silica tetrahedra, those with the ratio 1:3 contain chains of vertex-sharing silica tetrahedra, and KNAURSI with the ratio 1:4 contains sheets of silica tetrahedra. Thus, increasing Si relative to U results in increased polymerization of the silica tetrahedra. Also, the details of linkage between the silica and uranyl polyhedra are dependent on U:Si ratio. In soddyite, with a ratio of 2:1, each silica tetrahedron shares two of its edges with uranyl polyhedra, but in structures with the ratio 1:1, only one edge of each silica tetrahedron is shared with a uranyl polyhedron, and each tetrahedron links to another uranyl polyhedron by

vertex-sharing. In structures with a 1:3 ratio, some silica tetrahedra share a single edge with a uranyl polyhedron, whereas others do not share any polyhedral elements with uranyl polyhedra. Finally, in KNAURSI with the ratio 1:4, only vertex sharing occurs between uranyl polyhedra and silica tetrahedra, but all four equatorial vertices of the uranyl square bipyramids are shared with silica tetrahedra of adjacent sheets.

Plesko et al. [15] synthesized several uranyl silicates in sealed tubes at 200–300°C and 30 MPa, including weeksite and a K-uranyl silicate with a U:Si ratio close to that of KNAURSI (the 'NP phase'): $K_2O{\cdot}4UO_3{\cdot}15SiO_2$. Plesko et al. [15] performed their syntheses in a Na-free system, and the alkali content of their 'NP phase' is substantially less than that of KNAURSI. Comparing X-ray powder diffraction data reported by Plesko et al. [15] with both calculated and experimentally derived powder data for KNAURSI (Table 2) indicates that the phase synthesized by Plesko et al. [15] is structurally distinct from KNAURSI.

5. Discussion

KNAURSI was not observed until after the glass had reacted with water vapor at 200°C for 35 days. Crystals were commonly interspersed with other crystalline solids on the surface of the reacted glass, including sodium-bearing zeolites, and an acicular uranium silicate tentatively identified as weeksite. Other solid phases apparent on the surface of the altered glass after 35 days of reaction were calcium and iron phosphosilicates, calcium and iron silicates, and an alkali-bearing calcium silicate. Calcium hydroxide was also observed after 28 days of reaction, indicating the pH of the water film on the glass surface was relatively high at that point. After the appearance of KNAURSI, the amount of weeksite steadily decreased, and the size and quantity of crystals of KNAURSI increased.

Gong et al. [16,17] described alteration products formed on the surface of the French nuclear-waste glass, SON68, that had been exposed to a saturated vapor environment for up to 1021 days at 200°C. The only U-bearing alteration product on the surface of glass after 1021 days of reaction was reported to be weeksite [16,17]. Although they provide no analytical data, Gong et al. [17] reproduce an SEM micrograph of thinly bladed crystals that they identify as weeksite, which do not resemble crystals of KNAURSI (Fig. 1). The French SON68 glass has a similar, though slightly lower, total alkali content than 51S glass; however, SON68 contains no K (cf. Table 1 in Ref. [16]). The extreme durability of the SON68 glass compared with that of the 51S glass under nominally identical experimental conditions, as well as other compositional differences between these two glasses (e.g., Fe), suggest that KNAURSI does not form from the SON68 glass within the time frame described by Gong et al. [16]. However, as weeksite precipitated on the 51S glass before crystallization of KNAURSI, sufficiently long reaction times (>1021 days) might be expected to produce crystals of KNAURSI from a vapor-hydrated SON68 glass.

5.1. Potential radionuclide incorporation in KNAURSI

Burns et al. [10] discussed possible incorporation mechanisms of actinide elements into the structures of a variety of uranyl phases, including several uranyl silicates. The incorporation of actinides into phases that form due to the corrosion of nuclear waste in a geological repository is important because the secondary uranyl phases will become the near-field source material for actinides incorporated into their crystal structures. In the event that KNAURSI forms due to the corrosion of actinide-bearing waste glass in a geological repository, will it impact upon the release rates of radionucludes by the direct incorporation of actinides other than U into its crystal structure?

Consider first the incorporation of Np^{5+}. The crystal chemistry of Np^{5+} is discussed by Burns et al. [18], and is remarkably similar to U^{6+} in that the Np^{5+} cation typically occurs in structures as part of a nearly linear $(NpO_2)^+$ ion with Np–O bond-lengths ~0.18 nm. The neptunyl ion occurs in structures coordinated by four, five or six anions arranged at the equatorial corners of square, pentagonal and hexagonal bipyramids, in exactly the same fashion as the uranyl ion, except that the Np–O bond-lengths are slightly longer than the U–O bond-lengths in corresponding uranyl polyhedra. Thus, the prediction that Np will be incorporated into KNAURSI in place of U in the square bipyramids seems well-founded on the basis of the similar crystal chemistries of Np^{5+} and U^{6+}, provided that a suitable charge-balancing mechanism can also occur. Incorporation of a divalent or trivalent cation in the interstitial sites would provide a charge-balancing mechanism.

The incorporation of Pu^{4+} into the structure could only reasonably occur at the U^{6+} site. The Pu^{4+} cation tends to occur in a nearly holosymmetric octahedral coordination, and there is no plutonyl ion in the case of Pu^{4+} in crystal structures. The U^{6+} polyhedron in the structure of KNAURSI, although containing six anions, is strongly distorted owing to the presence of the uranyl ion. Incorporation of Pu^{4+} at the site would be inconsistent with the existing polyhedral geometry, and would require a substantially different distribution of bond valences within the polyhedron. Thus, it appears unlikely that Pu^{4+} will be incorporated into the structure of KNAURSI.

The incorporation of Am^{3+} is most feasible in the low-valence cation sites, as the cation is incompatible with either the U^{6+} or Si^{4+} sites. Polyhedral geometries

for Am^{3+} in known structures are summarized by Burns et al. [18], and typically involve from six to eight ligands at 0.235–0.255 nm. The substitution of Am^{3+} might occur at any of the K, Na(1), Na(2) or Na(3) sites in KNAURSI, although incorporation requires a charge-balancing substitution. Possible substitutions include Np^{5+} at the U^{6+} site or Al^{3+} in place of Si^{4+} in the tetrahedral sites.

Acknowledgements

This research was funded by the Environmental Management Sciences Program of the United States Department of Energy to PCB (DE-FG07-97ER14820). Financial support for RAO was provided by the US Department of Energy, Office of Environmental Management, under contract W-31-109-ENG-38. Electron microprobe analyses were performed in the Department of Geology, University of Western Ontario.

References

[1] R. Vochten, N. Blaton, O. Peeters, N. Jb. Mineral Mh. 1997 (12) (1997) 569.
[2] W.L. Ebert, J.K. Bates, W.L. Bourcier, Waste Manag. 11 (1991) 205.
[3] T.A. Abrajano Jr., J.K. Bates, J.J. Mazer, J. Non-Cryst. Solids 108 (1989) 269.
[4] J.K. Bates, L.J. Jardine, M.J. Steindler, Science 218 (1982) 51.
[5] J.K. Bates, M.G. Seitz, M.J. Steindler, Nucl. Chem. Waste Manag. 5 (1984) 63.
[6] R.H. Doremus, J. Non-Cryst. Solids 19 (1975) 137.
[7] C.A. Houser, J.S. Herman, I.S.T. Tsong, W.B. White, W.A. Lanford, J. Non-Cryst. Solids 41 (1980) 89.
[8] P.C. Burns, Can. Mineral. 36 (1998) 847.
[9] J.A. Ibers, W.C. Hamilton (Eds.), International Tables for X-ray Crystallography, vol. 4, 1974, Kynoch, Birmingham, UK.
[10] P.C. Burns, R.C. Ewing, F.C. Hawthorne, Can. Mineral. 35 (1997) 1551.
[11] H.T. Evans Jr., Science 141 (1963) 154.
[12] R.D. Shannon, Acta Crystallogr. A 32 (1976) 751.
[13] P.C. Burns, M.L. Miller, R.C. Ewing, Can. Mineral. 34 (1996) 845.
[14] F. Liebau, Structural Chemistry of Silicates, Springer, Berlin, 1985.
[15] E.P. Plesko, B.E. Scheetz, W.B. White, Am. Mineral. 77 (1992) 431.
[16] W.L. Gong, L.M. Wang, R.C. Ewing, E. Vernaz, J.K. Bates, W.L. Ebert, J. Nucl. Mater. 254 (1997) 249.
[17] W.L. Gong, R.C. Ewing, L.M. Wang, E. Vernaz, J.K. Bates, W.L. Ebert, Mater. Res. Soc. Symp. Proc. 412 (1996) 197.
[18] P.C. Burns, R.C. Ewing, M.L. Miller, J. Nucl. Mater. 245 (1997) 1.